Research Journal of Applied Sciences 1(1-4): 52-57, 2006

Electromagnetic Scattering Analysis of Structures: Application in Radar Systems

S. Redadaa, A. Boualleg and M. Benslama
Laboratoire d'Electromagnétisme et des Télécommunications,
Université de Constantine, Constantine 25000, Algérie

Abstract: Radar remote sensing deals with the extraction of object information from electromagnetic wave parameters. To fully exploit the potential of acquiring quantitative information requires a detailed description of the microwaves scattering. The research on this topic was mostly centered on far-field analysis which assume an incident plane wave, compute its scattered field and evaluate the Radar Cross Section (RCS). However, under certain practical conditions, the far-field analysis is not valid and a near-field analysis is necessary. In this paper, we present a full analysis of the near field of a wedge structure due to an incident wave field from a line source or a plane wave. The far field pattern, for the case of a line source exciting the structure, is also analyzed. Radar cross section of a rectangular flat plate is examined.

Key words: Electromagnetic wave, scattering, structure, radar cross section

INTRODUCTION

The problem of electromagnetic wave scattering is very important in many applications such remote sensing, antennas design and especially in defense applications. The study on this topic was mostly centered on far-field analysis which assume an incident plane wave, compute its scattered field due to the scatterer and evaluate the Radar Cross Section (RCS) of the scatterer. When the transmitting and receiving antennas are far from the scatterer, the incident wave can be approximated by a plane wave and the scattered far field can be regarded as the radiation far field due to the induced currents on the scatterer, the far-field analysis thus applies. However, in practical applications, there are many situations that the distance between the transmitting antenna and the scatterer is not large enough to treat the field arriving the scatterer as a plane wave and the relative motion between the antennas and scatterer will produce Doppler frequency shift. In these conditions the far-field analysis is not valid and a near-field analysis is necessary[1].

In calculating radar cross section of complex targets[2,3] some parts of the structure can be modeled using singly curved sheets, as for example the wings of an aircraft. For electrically large bodies the Geometrical Theory of Diffraction (GTD)[4,5] is a good high frequency technique for computing the scattering from those bodies. But, as it is well known, that method is not valid in the caustic of reflected rays which occurs for example when we illuminate by a plane wave a singly curved screen. Physical Optics (PO) has been largely used in the last years for predicting high frequency radar cross-section problems because, unlike Geometrical Optics and the GTD, is valid in the transition regions and at caustics. PO can be improved using the fringe currents contribution of the edge currents of the Physical Theory of Diffraction (PTD)[6,7].

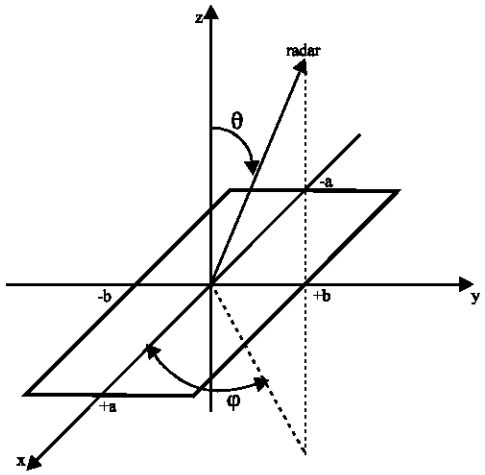

Fig. 1: Coordinates for rectangular flat plate

Scattering analysis: The RCS of a target characterizes its scattering property, which is defined as the area intercepting the amount of power that, when scattered isotropically, produces in a receiver a density that is equal to the density scattered by the actual target. When the transmitter and receiver are in the same location, the RCS is referred to as monostatic (or backscattered) and it is

Corresponding Author: Redadaa, S., Laboratoire d'Electromagnétisme et des Télécommunications, Université de Constantine, Constantine 25000, Algérie

referred to as bistatic when the two are located at different positions. For three-dimensional target, the RCS is given in terms of incident power density, magnetic field and electric field[8]. The RCS in terms of electric field is given by:

$$\sigma_{3-D} = \lim_{\rho\to\infty}\left[4\pi\rho^2\frac{\left|E^s\right|^2}{\left|E^i\right|^2}\right] \tag{1}$$

where ρ is the distance from target to observation point, E^S and E^i are scattered and incident electric field. The Eq. 1 is valid when the target is illuminated by a plane wave which in practice can be only approximated when the target is placed in the far field of the source, i.e. at least $\rho = 2D^2/\lambda$, where D is the largest dimension of the target.

Consider a perfectly conducting rectangular thin flat plate in the x-y plane as shown in Fig. 1. For a linearly polarized incident wave in the x-y plane, the horizontal and vertical backscattered radar cross section are, respectively, given by

$$\sigma_V = \frac{b^2}{\pi}\left|\sigma_{1V} - \sigma_{2V}\left[\frac{1}{\cos\theta} + \frac{\sigma_{2V}}{4}\left(\sigma_{3V}+\sigma_{4V}\right)\sigma_{5V}^{-1}\right]\right|^2 \tag{2}$$

$$\sigma_H = \frac{b^2}{\pi}\left|\sigma_{1H} - \sigma_{2H}\left[\frac{1}{\cos\theta} - \frac{\sigma_{2H}}{4}\left(\sigma_{3H}+\sigma_{4H}\right)\sigma_{5H}^{-1}\right]\right|^2 \tag{3}$$

where

$$\begin{aligned}
\sigma_{1V} &= \cos\left(k_a\sin\theta\right) - j\frac{\sin\left(k_a\sin\theta\right)}{\sin\theta}\\
\sigma_{2V} &= \frac{e^{j(ka-\pi/4)}}{\sqrt{2\pi}\left(k_a\right)^{3/2}} \quad \sigma_{3V} = \frac{\left(1+\sin\theta\right)e^{-jk_a\sin\theta}}{\left(1-\sin\theta\right)^2}\\
\sigma_{4V} &= \frac{\left(1-\sin\theta\right)e^{jk_a\sin\theta}}{\left(1+\sin\theta\right)^2} \quad \sigma_{5V} = 1 - \frac{e^{j(2k_a-\pi/2)}}{8\pi\left(k_a\right)^3}
\end{aligned} \tag{4}$$

$$\begin{aligned}
\sigma_{1H} &= \left(\sigma_{1V}\right)^* \quad \sigma_{2H} = \frac{4e^{j(k_a+\pi/4)}}{\sqrt{2\pi}\left(k_a\right)^{1/2}}\\
\sigma_{3H} &= \frac{e^{-jk_a\sin\theta}}{1-\sin\theta} \quad \sigma_{4H} = \frac{e^{jk_a\sin\theta}}{1+\sin\theta}\\
\sigma_{5H} &= 1 - \frac{e^{j(2k_a+\pi/2)}}{2\pi\left(k_a\right)}
\end{aligned} \tag{5}$$

wherein $k_a = k_0 a$, k_0 is the free space wave number. Equation 2 and 3 are valid quite accurate for aspect angles

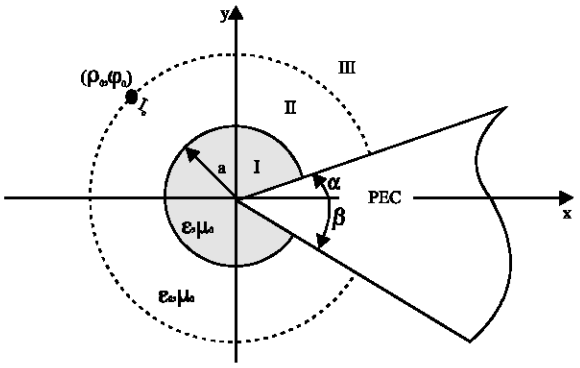

Fig. 2: Capped wedge structure

$0° \le \theta \le 80°$. For aspect angles near 90°, Ross[9] obtained by extensive fitting of measured data an empirical expression for the radar cross section. It is given by

$$\begin{aligned}
&\sigma_H \to 0\\
&\sigma_V = \frac{ab}{\lambda}\left\{\left[1+\frac{\pi}{2\left(2a/\lambda\right)^2}\right] + \left[1-\frac{\pi}{2\left(2a/\lambda\right)^2}\right]\cos\left(2k_a - \frac{3\pi}{5}\right)\right\}
\end{aligned} \tag{6}$$

The backscattered RCS for a perfectly conducting thin rectangular plate for incident waves at any θ, φ can be approximated by:

$$\sigma = \frac{4\pi a^2 b^2}{\lambda^2}\left(\frac{\sin\left(ak_0\sin\theta\cos\varphi\right)}{ak_0\sin\theta\cos\varphi}\,\frac{\sin\left(bk_0\sin\theta\cos\varphi\right)}{bk_0\sin\theta\cos\varphi}\right)^2\left(\cos\theta\right)^2 \tag{7}$$

Equation 7 is independent of the polarization and it is only valid for aspect angles $\theta \le 20°$. The goal of analysis is to find the field expressions for the problem of scattering by a two-dimensional (2-D) Perfect Electric Conduction (PEC) wedge capped with a dielectric cylinder (Fig. 2). Using the cylindrical coordinates system, the excitation due to an electric line current of amplitude I_e located at (ρ_0, φ_0) result in Transverse Magnetic (TM) incident field with the electric field expression given by

$$E_z^i = -I_e\frac{\omega\mu_0}{4}H_0^{(2)}\left(k_0\left|\rho-\rho_0\right|\right) \tag{8}$$

where $H_0^{(2)}$ is the Hankel function of the second kind of order zero.

The problem is divided into three regions I, II and III. The field expressions may be assumed to take the following forms:

$$\begin{aligned}
E_z^I &= \sum_{n=0}^{\infty} a_n J_v(k_1\rho)\sin v(\varphi-\alpha)\sin v(\varphi_0-\alpha)\\
E_z^{II} &= \sum_{n=0}^{\infty}\left(b_n J_v(k_0\rho)+c_n H_v^{(2)}(k_0\rho)\right)\sin v(\varphi-\alpha)\sin v(\varphi_0-\alpha)\\
E_z^{III} &= \sum_{n=0}^{\infty} d_n H_v^{(2)}(k_0\rho)\sin v(\varphi-\alpha)\sin v(\varphi_0-\alpha)
\end{aligned} \tag{9}$$

where k_1 is the wave number inside the dielectric.

$$v=\frac{n\pi}{2\pi-\alpha-\beta} \tag{10}$$

while $J_v(x)$ and $H_v^{(2)}$ are the Bessel and Hankel functions of order v and argument x. From Maxwell equations, the magnetic field component H_φ is related to the electric field component E_z for a TMwave by

$$H_\varphi=\frac{1}{j\omega\mu}\frac{\partial E_z}{\partial\rho} \tag{11}$$

Thus, the magnetic field component H_φ in the various regions may be written as

$$\begin{aligned}
H_\varphi^I &= \frac{k_1}{j\omega\mu_0}\sum_{n=0}^{\infty} a_n J_v'(k_1\rho)\sin v(\varphi-\alpha)\sin v(\varphi_0-\alpha)\\
H_\varphi^{II} &= \frac{k_0}{j\omega\mu_0}\sum_{n=0}^{\infty}\left(b_n J_v'(k_0\rho)+c_n H_v^{(2)'}(k_0\rho)\right)\sin v\\
&\quad (\varphi-\alpha)\sin v(\varphi_0-\alpha)\\
H_\varphi^{III} &= \frac{k_0}{j\omega\mu_0}\sum_{n=0}^{\infty} d_n H_v^{(2)'}(k_0\rho)\sin v(\varphi-\alpha)\sin v(\varphi_0-\alpha)
\end{aligned} \tag{12}$$

where the prime indicated derivatives with respect to the full argument of the function. The boundary conditions require that he tangential electric field components vanish at the PEC surface. Also the tangential field components should be continuous across the air-dielectric surface and the virtual boundary between regions I and II, except for the discontinuity of the magnetic field at the source point. Thus,

$$E_z=0 \text{ at } \varphi=\alpha, 2\pi-\beta \tag{13}$$

$$\begin{cases} E_z^I = E_z^{II} \\ H_\varphi^I = H_\varphi^{II} \end{cases} \text{ at } \rho=a \tag{14}$$

$$\begin{cases} E_z^{II} = E_z^{III} \\ H_\varphi^{II} = H_\varphi^{III} \end{cases} \text{ at } \rho=\rho_0 \tag{15}$$

The current density J_e may be given in Fourier series expansion as:

$$\begin{aligned}
J_e &= \frac{I_e}{\rho_0}\delta(\varphi-\varphi_0)=\frac{2}{2\pi-\alpha-\beta}\frac{I_e}{\rho_0}\\
&\sum_{n=0}^{\infty}\sin v(\varphi-\alpha)\sin v(\varphi_0-\alpha)
\end{aligned} \tag{16}$$

The boundary condition on the PEC surface is automatically satisfied by the φ dependence of the electric field Eq. 9. From the boundary conditions in Eq. 14

$$\begin{aligned}
&\sum_{n=0}^{\infty} a_n J_v(k_{1a})\sin v(\varphi-\alpha)\sin v(\varphi_0-\alpha)=\\
&\sum_{n=0}^{\infty}\left(b_n J_v(k_a)+c_n H_v^{(2)}(k_a)\right)\sin v(\varphi-\alpha)\sin v(\varphi_0-\alpha)
\end{aligned} \tag{17}$$

$$\begin{aligned}
&\frac{k_1}{j\omega\mu_0}\sum_{n=0}^{\infty} a_n J_v'(k_{1a})\sin v(\varphi-\alpha)\sin v(\varphi_0-\alpha)=\frac{k_0}{j\omega\mu_0}\\
&\sum_{n=0}^{\infty}\left(b_n J_v'(k_a)+c_n H_v^{(2)'}(k_a)\right)\sin v(\varphi-\alpha)\sin v(\varphi_0-\alpha)
\end{aligned} \tag{18}$$

From the boundary conditions in Eq. 15, we have

$$\begin{aligned}
&\sum_{n=0}^{\infty}\left(b_n J_v(k_0\rho_0)+c_n H_v^{(2)}(k\rho_0)\right)\sin v(\varphi-\alpha)\sin v(\varphi_0-\alpha)\\
&=\sum_{n=0}^{\infty} d_n H_v^{(2)}(k_0\rho_0)\sin v(\varphi-\alpha)\sin v(\varphi_0-\alpha)
\end{aligned} \tag{19}$$

$$\begin{aligned}
&\frac{k}{j\omega\mu_0}\sum_{n=0}^{\infty}\left(b_n J_v'(k_0\rho_0)+c_n H_v^{(2)'}(k_0\rho_0)\right)=\\
&\frac{k}{j\omega\mu_0}\sum_{n=0}^{\infty}\sin v(\varphi-\alpha)\sin v(\varphi_0-\alpha)\\
&\frac{k}{j\omega\mu_0}\sum_{n=0}^{\infty} d_n H_v^{(2)'}(k_0\rho_0)\sin v(\varphi-\alpha)\sin v(\varphi_0-\alpha)\\
&-\frac{2}{2\pi-\alpha-\beta}\frac{I_e}{\rho_0}\sum_{n=0}^{\infty}\sin v(\varphi-\alpha)\sin v(\varphi_0-\alpha)
\end{aligned} \tag{20}$$

Since Eq. 17 and 20 hold for all φ, the series of the left and right hand sides be equal term by term, more precisely,

$$a_n J_v(k_{1a})=b_n J_v(k_a)+c_n H_v^{(2)}(k_a) \tag{21}$$

$$k_1 a_n J_v'(k_{1a}) = k\left(b_n J_v'(k_a) + c_n H_v^{(2)'}(k_a)\right) \quad (22)$$

$$b_n J_v(k_0\rho_0) + c_n H_v^{(2)}(k_0\rho_0) = d_n H_v^{(2)}(k_0\rho_0) \quad (23)$$

$$b_n J_v'(k\rho_0) + c_n H_v^{(2)'}(k\rho_0) = d_n H_v^{(2)'}(k\rho_0) - \frac{2j\eta_0}{2\pi-\alpha-\beta}\frac{I_e}{\rho_0} \quad (24)$$

where η_0 is the characteristic impedance of free space. From Eq. 21 and 23, we have

$$a_n = \frac{1}{J_v(k_{1a})}\left[b_n J_v(k_a) + c_n H_v^{(2)}(k_a)\right] \quad (25)$$

$$d_n = c_n + b_n \frac{J_v(k_0\rho_0)}{H_v^{(2)}(k_0\rho_0)} \quad (26)$$

After some mathematical operations, we get

$$b_n = -\frac{\pi\omega\mu_0 I_e}{2\pi-\alpha-\beta} H_v^{(2)}(k_0\rho_0) \quad (27)$$

Substituting b_n in Eq. 21 and 22 and solving for c_n yield

$$c_n = \frac{\pi\omega\mu_0 I_e}{2\pi-\alpha-\beta}\left[\begin{array}{l} H_v^{(2)}(k_0\rho_0) \\ \dfrac{kJ_v'(k_a)J_v(k_{1a}) - k_1 J_v(ka) J_v'(k_{1a})}{k_0 H_v^{(2)'}(k_a)J_v(k_{1a}) - k_1 H_v^{(2)}(k_a)J_v'(k_{1a})} \end{array}\right] \quad (28)$$

From Eq. 26 through 28, d_n may be given by

$$d_n = \frac{\pi\omega\mu_0 I_e}{2\pi-\alpha-\beta}\left[\begin{array}{l} H_v^{(2)}(k_0\rho_0) \\ \dfrac{k_0 J_v'(k_a)J_v(k_{1a}) - k_1 J_v(k_a) J_v'(k_{1a})}{kH_v^{(2)'}(k_a)J_v(k_{1a}) - k_1 H_v^{(2)}(k_a)J_v'(k_{1a})} \\ -J_v(k_0\rho_0) \end{array}\right] \quad (29)$$

with these closed form expressions for the expansion coefficients a_n, b_n, c_n and d_n, the field components E_z and H_φ can be determined from Eq. 9 and Eq. 12, respectively. Alternatively, the magnetic field component H_ρ can be computed from

$$H_\rho = -\frac{1}{j\omega\mu}\frac{1}{\rho}\frac{\partial E_z}{\partial\varphi} \quad (30)$$

Thus, the H_ρ expressions for the three regions defined in Fig. 2 become

$$\begin{aligned} H_\rho^{I} &= -\frac{1}{j\omega\mu\rho}\sum_{n=0}^{\infty} a_n v J_v(k_1\rho)\cos v(\varphi-\alpha)\sin v(\varphi_0-\alpha) \\ H_\rho^{II} &= -\frac{1}{j\omega\mu\rho}\sum_{n=0}^{\infty} v\left(b_n J_v(k_0\rho) + c_n H_v^{(2)}(k_0\rho)\right)\cos v(\varphi-\alpha)\sin v(\varphi_0-\alpha) \\ H_\rho^{III} &= -\frac{1}{j\omega\mu\rho}\sum_{n=0}^{\infty} d_n v H_v^{(2)}(k_0\rho)\cos v(\varphi-\alpha)\sin v(\varphi_0-\alpha) \end{aligned} \quad (31)$$

In region III, the far scattered field may be found as the difference between the total and incidents field. Thus, using Eq. 8 and 9 and considering the far field condition ($\rho\to\infty$) we get

$$\begin{aligned} E_z^{III} &= E_z^i + E_z^s = \sqrt{\frac{2j}{\pi k_0\rho}} e^{-jk\rho} \\ &\sum_{n=0}^{\infty} d_n j^v \sin v(\varphi-\alpha)\sin v(\varphi_0-\alpha) \end{aligned} \quad (32)$$

For plane wave excitation ($\rho_0\to\infty$), the expressions in Eq. 27 and 28 reduce to

$$b_n = -\frac{\pi\omega\mu_0 I_e}{2\pi-\alpha-\beta} j^v \sqrt{\frac{2j}{\pi k_0\rho_0}} e^{-jk_0\rho_0} \quad (33)$$

$$c_n = \frac{\pi\omega\mu_0 I_e}{2\pi-\alpha-\beta} j^v \sqrt{\frac{2j}{\pi k_0\rho_0}} e^{-jk_0\rho_0} \frac{k_0 J_v'(k_a)J_v(k_{1a}) - k_1 J_v(k_a) J_v'(k_{1a})}{k_0 H_v^{(2)'}(k_a)J_v(k_{1a}) - k_1 H_v^{(2)}(k_a)J_v'(k_{1a})} \quad (34)$$

where the complex of the incident plane wave, E_0, can be given by:

$$E_0 = -I_e \frac{\omega\mu_0}{4}\sqrt{\frac{2j}{\pi k\rho_0}} e^{-jk_0\rho_0} \quad (35)$$

in this study, the field components can be evaluated in regions I and II only.

RESULTS AND DISCUSSION

Figure 3 presents the radar cross section of a rectangular flat plate for the vertical and horizontal polarizations, compared with the classical formulae. The parameters of structure are a = b = 10.16 cm and f = 300MHz.

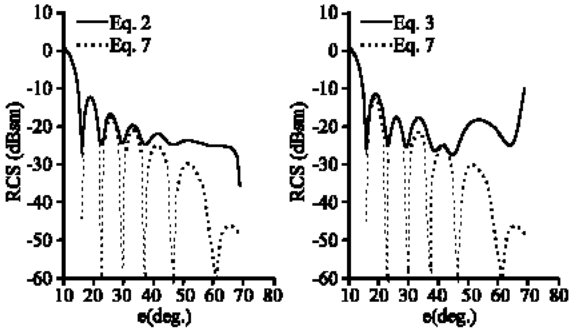

Fig. 3: Backscattered RCS for a rectangular flat plate (a) Vertical polarization (b) horizontal polarization

Figure 4 presents the far field of a capped wedge in the presence of an electric line source field. We clearly show how the cap parameters affect the maximum radiation of the line source in the presence of wedge. The distribution of the components of the fields on the near field of two cases (conducting capped edge, dielectric capped edge) is computed and shown in Fig. 5 and 6. The near field distribution for an incident wave field of the two types of wedges is also computed and shown in Fig. 7 and 8. These near field distributions clearly demonstrated the effect of cap parameters in altering the sharp edge

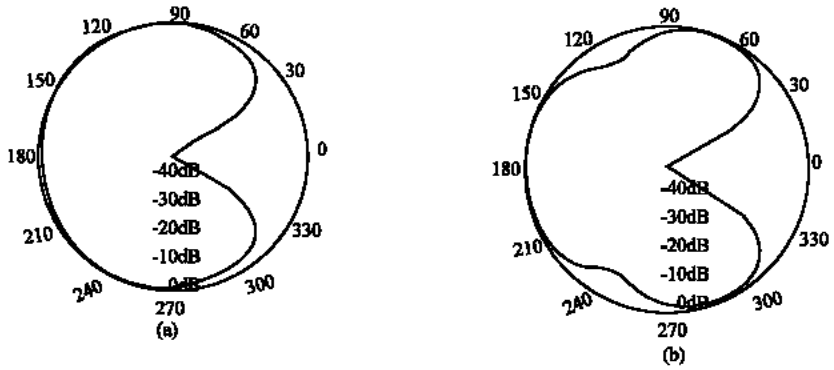

Fig. 4: Total far field pattern of a line source near a conducting wedge (a) conducting-capped edge (b) dielectric-capped edge

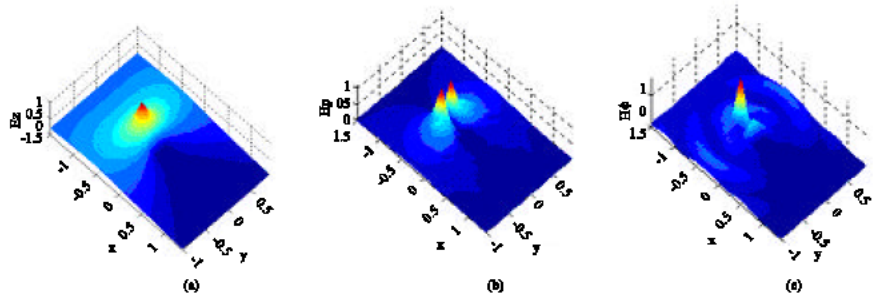

Fig. 5: Near field patterns of a line source near a conducting wedge with conducting-capped edge (a)E_z (b) H_ρ (c)H_ϕ

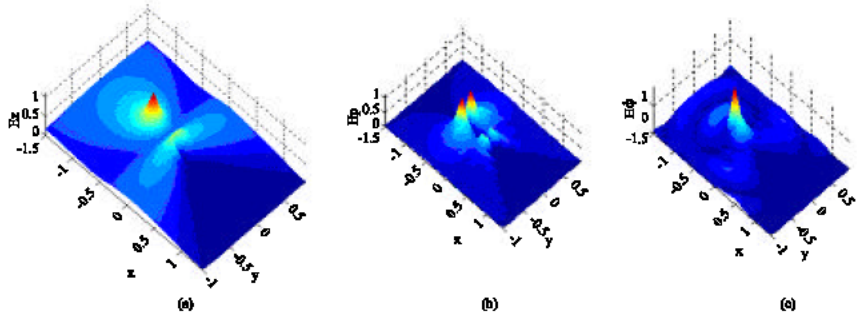

Fig. 6: Near field patterns of a line source near a conducting wedge with dielectric-capped edge (a)E_z (b) H_ρ (c)H_ϕ

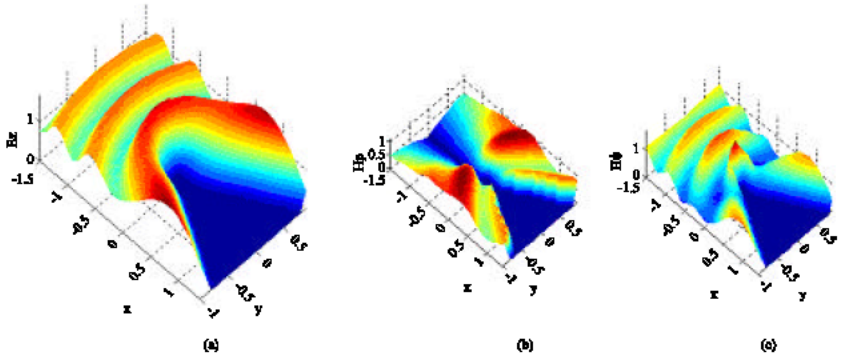

Fig. 7: Near field patterns of plane wave incident on a conducting wedge with conducting-capped edge (a)E_z (b) H_ρ (c)H_ϕ

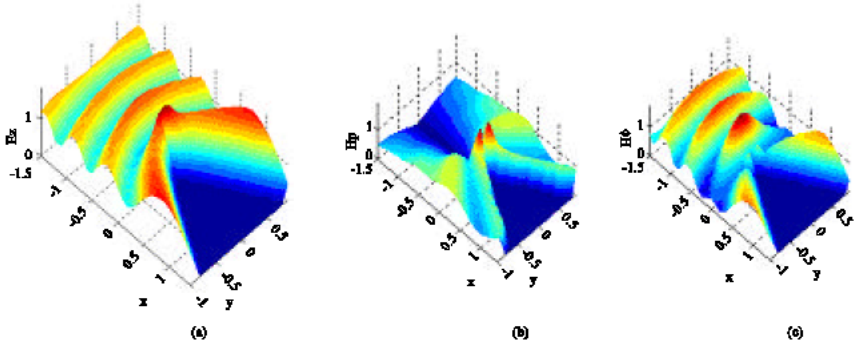

Fig. 8: Near field patterns of plane wave incident on a conducting wedge with dielectric-capped edge (a)E_z (b) H_ρ (c)H_ϕ

singular behaviour. We have used the following wedge structure parameters:.

$$a = 0.15m, \rho_0 = 0.5m, \alpha = \beta = 30^\circ, \varepsilon_r = 3, I_e = 1mA$$

CONCLUSION

In this study, we have presented a full analysis of electromagnetic scattering. We have presented a case of backscattered radar cross section for a rectangular flat plate. An analysis of the far and near field patterns for a wedge structure shows the effect of cap parameters on the maximum radiation of the line source. We have also examined the effect the cap parameters on the sharp edge behavior for an incident plane wave.

REFERENCES

1. Jeng, S.K., 1998. Near-field scattering by physical theory of diffraction and shooting and bouncing rays, IEEE Trans. Ant. Propag., 46: 551-558.
2. Youssef, N.N., 1989. Radar cross section of complex targets. Proc. IEEE, 77: 722-734.
3. Colton, D. and R. Kress, 1983. Integral Eqn. Methods in scattering theory. John Wiley, New York.
4. Kouyoumjian, R.G. and P.H. Pathak, 1974. A uniform geometrical theory of diffraction for an edge in a perfectly conducting surface. Proc. IEEE, 62: 1448-1461.
5. Rao, S., D. Wilton and A. Glisson, 1982. Electromagnetic scattering by surfaces of arbitrary shape. IEEE Trans. Ant. Propag., 30: 409-418.
6. Knott, E.F., J.F. Shaeffer and M.T. Tuley, 1985. Radar cross section: Its prediction, measurement and reduction. Dedham, MA: Artech House.
7. Blume, S. and V. Krebs, 1998. Numerical evaluation of dyadic diffraction coefficients and bistatic radar cross sections for a perfectly conducting semi-infinite elliptic cone. IEEE Trans. Ant. Propag., 46: 414-424.
8. Balanis, C.A., 1997. Antenna Theory: Analysis and Design. John Wiley and Sons, 2nd Edn., New York .
9. Ross, A., 1966. Radar cross section of rectangular flat plate as function of aspect angle. IEEE Trans. Ant. Propag., 14: 329-335.